JOURNAL OF PROPULSION AND POWER
Vol. 12, No. 6, November–December 1996

Expansion Corner Effects on Hypersonic Shock Wave/Turbulent Boundary-Layer Interactions

Michael E. White* and David A. Ault†
Johns Hopkins University, Applied Physics Laboratory, Laurel, Maryland 20723-6099

An experimental program has been conducted to investigate the behavior of hypersonic shock wave/turbulent boundary-layer interactions in the vicinity of an expansion corner. Tests were run in the Calspan 96-in. shock tunnel at nominal Mach 11.5 freestream conditions for a unit Reynolds number of approximately 18 × 10^6/ft. Fully turbulent boundary layers were generated with a flat plate, and oblique shocks were generated with a planar shock generator canted at angles of 10, 12, and 15 deg relative to the freestream. Shock-impingement points were varied to create impingement points upstream, in the vicinity, and downstream of an expansion corner with an angle that was similar in magnitude to the shock generator. Wall static pressure and heat transfer were measured in the region of the shock interaction to determine the effects of the expansion corner on the character of the shock wave/boundary-layer interaction. Detailed data have been generated for comparison with computational codes and to enable a better understanding of hypersonic inlet design.

Introduction

A RESURGENCE in research interest relating to hypersonic aerodynamics and propulsion came about in 1986 as a result of the National Aerospace Plane (NASP) program. The NASP program objectives included development and demonstration of the enabling technologies required to achieve single-stage-to-orbit (SSTO) flight with a horizontal takeoff and landing vehicle powered by air-breathing engines. These technologies varied from advanced tires to handle the high projected takeoff speeds to advanced materials capable of withstanding the high heat transfer, high shear, oxidizing environment in a scramjet combustor. One of the most important technology requirements is related to the development and demonstration of advanced propulsion technology to permit the use of air-breathing, dual-mode ramjet/scramjet engines for the main portion of the accelerator trajectory.

The design of a viable air-breathing engine for an SSTO vehicle requires an engine flow path that is fully integrated into the vehicle. A schematic diagram of an SSTO vehicle design is shown in Fig. 1. In such a design the entire underside of the vehicle is part of the propulsion flow path. The forward portion of the airframe acts as the initial inlet compression surface and the aft portion of the airframe acts as the nozzle expansion surface. Freestream air is compressed by the vehicle forebody and then captured by the inlet. The inlet further compresses the flow and directs it into the combustor through an internal shock system. In the combustor, fuel is mixed with the captured air and burned, and the effluent is expanded through the nozzle to generate vehicle thrust.

While conceptually very simple, there are many technical challenges associated with the development of a dual-mode ramjet/scramjet that can operate over the wide range of flight conditions typical of the air-breathing portion of an SSTO trajectory (approximately between Mach 3–18). A description of the operating features of a dual-mode ramjet engine for SSTO application is presented in Ref. 1 along with a description of some of the critical technical issues. Of principal interest in this effort is the operation of the scramjet inlet at high hypersonic flight speeds, and, in particular, a better understanding of shock wave/boundary-layer interactions (SWBLIs) typical of those inlets.

As an SSTO vehicle accelerates to hypersonic flight speeds, the flowfield structure for a typical planar engine design is shown in Fig. 2. The vehicle forebody compresses the freestream air through an initial oblique shock wave. This is followed by additional isentropic compression to the cowl lip. The total forebody turning is generally between 10–15 deg for typical SSTO vehicle designs. The cowl captures the forebody flowfield and provides additional compression through a shock wave that turns the flow back into the combustor, which is generally nearly aligned with the vehicle waterline. The isolator, located between the inlet shoulder and the start of combustion, stabilizes a precombustion shock system consistent with the pressure rise because of the heat release in the combustor. As the Mach number increases, the heat release in the combustor relative to the freestream total enthalpy decreases, reducing the pressure rise caused by combustion and the strength of the precombustion shock system. At a very high Mach number the precombustion shock system is eliminated and the shock structure in the engine is dominated by the shocks generated in the inlet.

The objective of a good inlet design is to provide the combustor with air that has been compressed as efficiently as possible to a level that permits efficient combustion. One potential design option is to design an inlet geometry that operates with the cowl shock canceled at the inlet shoulder. This design pro-

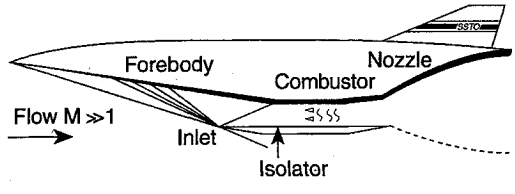

Fig. 1 Schematic diagram of an air-breathing SSTO vehicle.

Presented as Paper 95-6125 at the AIAA 6th International Aerospace Plane and Hypersonics Technologies Conference, Chattanooga, TN, April 3–7, 1995; received June 10, 1995; revision received April 26, 1996; accepted for publication April 29, 1996.

*Principal Staff, Aeronautics Department. Senior Member AIAA.
†Senior Staff, Aeronautics Department. Member AIAA.

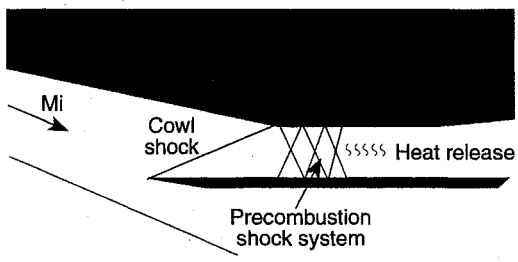

Fig. 2 Inlet flowfield schematic diagram for a dual-mode ramjet.

vides the combustor a flowfield with minimal nonuniformity and avoids compressing the flow, expanding, and then recompressing. However, true shock cancellation can only be achieved in the inviscid limit. For air-breathing SSTO vehicle designs, the long forebody results in an inlet capture flowfield that has a boundary-layer thickness that is typically 20% of the cowl height. As a result, the interaction of the cowl shock with the boundary layer that has formed on the vehicle forebody is of critical importance in determining actual inlet performance and operability.

This article presents the results of an experimental test program conducted to investigate the interaction between a fully turbulent boundary layer and an oblique shock wave in the vicinity of an expansion corner at a high hypersonic Mach number. Detailed data have been generated for comparison with computational codes and to enable a better understanding of hypersonic inlet design.

Previous Work

Previous work in the area of SWBLIs has been plentiful, and the references are too numerous to include in this article. Fortunately, there have been several survey papers to review these activities.[2,3] The overwhelming majority of the data generated for high-speed flow has been for geometries that include 1) a flat-plate boundary layer entering a compression corner, 2) oblique reflected shocks on a flat plate boundary layer, 3) three-dimensional glancing interactions on a flat plate boundary layer, and 4) flows over forward- and rearward-facing steps.

The problem of SWBLIs in the vicinity of an expansion corner was investigated[4,5] at Mach numbers of 1.8 and 2.5. Tests were run using a 6-deg expansion corner and shock-generator angles of 4, 6, and 8 deg. Experimental data were generated for a turbulent boundary layer developed on the wall of a supersonic blowdown wind tunnel. The principal conclusion of this effort was that the expansion corner effect was felt by an upstream interaction region when the interaction occurred less than 3–4 boundary-layer heights from the corner.

A test program to investigate SWBLIs at hypersonic speeds was performed by Hawbolt et al.[6] in the University of Toronto Institute for Aerospace Studies Mach 8 gun tunnel. Initial efforts to investigate turbulent boundary layers were unsuccessful because of facility Reynolds number limitations; therefore, this work was completed by evaluating the laminar boundary-layer interaction. Wall pressure data were generated for shock impingement on a laminar flat plate boundary layer for shock-generator angles of 2.6, 5.1, 7.4, and 10.0 deg, and it was determined that separation occurred for all shock-generator angles tested above 2.6 deg. The effect of an expansion corner was evaluated for shock-generator/expansion corner angles of 5 and 10 deg. Shock impingement points ranged from well upstream to well downstream of the corner. They found that when an interaction causes separation, the extent of separation is not affected by the expansion corner if it is fully contained either upstream or downstream of the corner, and the separation can be reduced or eliminated if it straddles the corner.

Attempts to evaluate the effects of an expansion corner on shock wave/turbulent boundary-layer interactions in hypersonic flow were made by Chung and Lu[7] using a Mach 8 shock tunnel at the University of Texas at Arlington. Evaluation of their results indicates that they suffered from facility Reynolds number limitations similar to those that plagued Hawbolt et al.[6]; however, in this work no effort was made to focus on a laminar boundary layer. As a result, the data presented in Ref. 7 are for a boundary layer that is transitional, and the interpretation of the results is, at best, very difficult because of the unsteady and nonrepeatable nature of transition.

Frew et al.[8] performed an extensive experimental evaluation of the interactions between shock waves and both laminar and turbulent boundary layers for a range of Reynolds numbers. Tests were run in the Mach 6 continuous flow tunnel at Wright Laboratory. Initial tests were for a flat plate with the shock-generator angle varied in increments of 0.2 deg to determine the angle of incipient separation. Data were then generated with sharp and rounded expansion corners, with single- and double-wedge shock generators, and with and without sidewalls. This database is the most relevant to the results described herein.

The database described herein provides information on the SWBLI at very high hypersonic Mach numbers and for a very high Reynolds number. The boundary layer is fully turbulent well ahead of the interaction region. Detailed heat transfer and pressure information have been generated for an interaction in the vicinity of an expansion corner for geometries typical of air-breathing SSTO inlet designs.

Experimental Apparatus

A wind-tunnel test program has been completed in the Calspan 96-in. shock tunnel at approximately Mach 11.5 flow conditions for a unit Reynolds number of approximately 18×10^6/ft. A schematic diagram of the experimental rig, a modified version of the rig tested without an expansion corner in Ref. 9, is shown in Fig. 3. It consists of a sharp, flat plate followed by an adjustable angle expansion surface. The shock generator is a sharp flat plate that is adjustable in angle, axial location, and vertical location. The model width was chosen consistent with that required to ensure two-dimensional flow at the centerline in the work of Ref. 9. Tests were run for shock-generator/expansion corner angles of 10, 12, and 15 deg to evaluate flow conditions corresponding to increasing regions of

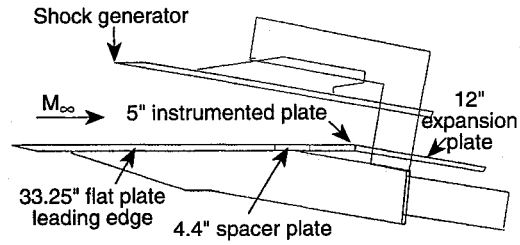

Fig. 3 Schematic diagram of the SWBLI model.

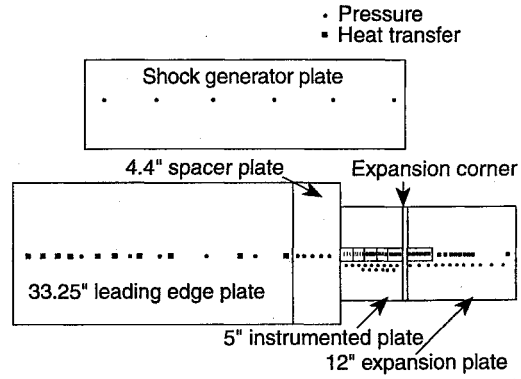

Fig. 4 Instrumentation layout on the SWBLI model.

Table 1 Model parameters and test conditions

Run	Mach no.	Re, 10^7/ft	Model configuration	θ_{attack}	θ_{roll}	$\theta_{S.G.}$	θ_{exp}	Shock-generator position, in. X	Y
2	11.54	1.783	I	—	—	—	—	—	—
3	11.55	1.657	I	—	—	—	—	—	—
4	11.54	1.823	I	—	—	—	—	—	—
6	11.54	1.779	II	3′	0′	12°14′	12°30′	−25.10	7.25
7	11.55	1.666	II	4′	0′	12°14′	12°30′	−28.87	8.06
8	11.54	1.773	II	3′	0′	12°15′	12°30′	−21.96	6.62
9	11.54	1.608	II	4′	−1′	12°30′	12°30′	−18.81	5.95
10	11.54	1.715	II	3′	0′	12°17′	12°33′	−28.87	8.08
11	11.56	1.801	II	3′	−1′	14°40′	15°03′	−28.03	9.07
12	11.55	1.813	II	4′	−3′	14°40′	15°03′	−18.22	6.56
13	11.54	1.843	II	4′	−3′	09°33′	10°00′	−30.00	6.96
14	11.54	1.759	II	3′	0′	09°33′	10°00′	−25.13	6.18
15	11.54	1.678	II	3′	0′	09°33′	10°00′	−21.52	5.60
16	11.55	1.777	II	3′	0′	09°46′	10°00′	−18.81	5.15
17	11.49	1.631	II	3′	−2′	14°50′	15°00′	−22.97	7.78
18	11.55	1.777	II	3′	0′	14°40′	15°00′	−14.50	6.23
20	11.55	1.805	II	3′	0′	14°45′	15°00′	−19.30	7.51
21	11.55	1.735	II	4′	0′	12°05′	12°33′	−20.00	6.43
22	11.55	1.822	II	4′	0′	12°02′	12°33′	−16.94	5.80
23	11.55	1.716	II	4′	0′	12°10′	12°33′	−15.42	5.49
24	11.55	1.836	II	4′	0′	12°10′	12°33′	−20.00	6.31

flow separation. Data were obtained for shock impingement well upstream, in the vicinity, and well downstream of the expansion corner where the impingement location is defined as the point of the initial shock induced pressure rise. The interaction region was characterized with wall static pressure and wall heat transfer data, and the inflow boundary layer was characterized at the expansion corner station using pitot rakes. Schlieren photographs were taken for flow visualization. A schematic of the surface instrumentation is shown in Fig. 4.

Model parameters and test conditions for the various runs are shown in Table 1. Model configuration I refers to the flat plate calibration runs, and II refers to the shock interaction runs. The flat plate angle of attack and roll angle are listed as θ_{attack} and θ_{roll}, respectively, and the shock-generator and expansion surface angles are listed as $\theta_{S.G.}$ and θ_{exp}, respectively. The location of the shock-generator leading edge relative to the expansion corner is also listed.

Results

Initial runs were made with only the flat plate installed in the tunnel to ensure that the boundary layer was fully turbulent and to permit characterization of the boundary layer at the expansion corner. Static pressure and heat transfer were measured on the flat plate to allow quantification of the location of boundary-layer transition.

Figure 5 shows a plot of heat transfer as a function of axial station on the flat plate, with the zero coordinate being the location of the expansion corner. As indicated in the figure, transition starts approximately 37 in. upstream of the expansion corner and is completed in approximately 7 in. Two pitot pressure rakes were installed to measure the boundary-layer profile and to permit calibration of the inviscid flow over the flat plate (Fig. 6). Figure 7 is a plot of the velocity distribution on the flat plate. It indicates that the boundary layer at the expansion corner is approximately 0.7 in. thick. It is pointed out here that the expansion corner is approximately 45 boundary-layer thicknesses downstream of the end of boundary-layer transition on the flat plate.

Upon completion of the flat plate calibration runs, the shock generator was installed and tests were run for nominal shock angles of 10, 12, and 15 deg. These three angles were chosen to span the range of cowl shock angles for typical SSTO inlet configurations. The location of the shock generator was varied for each of the shock angles such that the shock impingement point was swept across the expansion corner. Initial shock positions were determined from pretest calculations, and subsequent adjustments were made on the basis of an assessment of the initial data. For each shock-generator angle, initial tests were conducted with the shock impingement point sufficiently far forward to result in the full reflected shock pressure rise prior to the expansion corner.

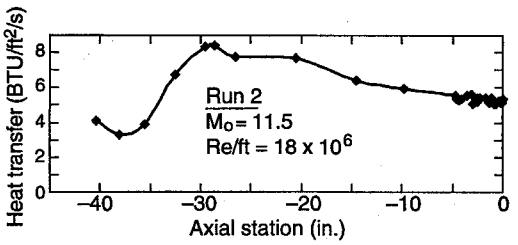

Fig. 5 Axial heat transfer distribution for the flat plate.

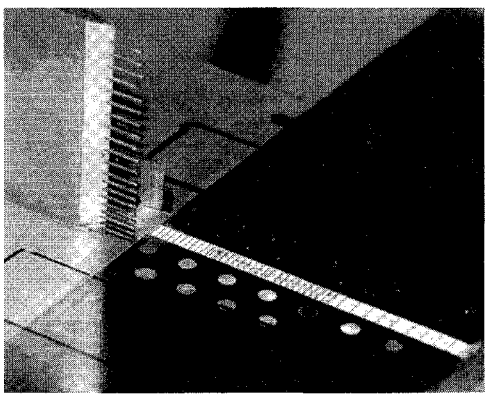

Fig. 6 Pitot rake installation at the expansion corner.

The pressure distributions for tests of the 10-deg shock generator are shown in Fig. 8. The most forward shock location resulted in a reflected shock pressure ratio of approximately 35:1, with the onset of the pressure rise occurring approximately 5 in. upstream of the expansion corner. As the shock position was moved aft, the maximum pressure rise was gradually decreased until the shock is effectively canceled at the shoulder. Note that for all of the shock positions tested, the static pressure downstream of the shoulder approaches the same value; however, the total pressure recovery of the various

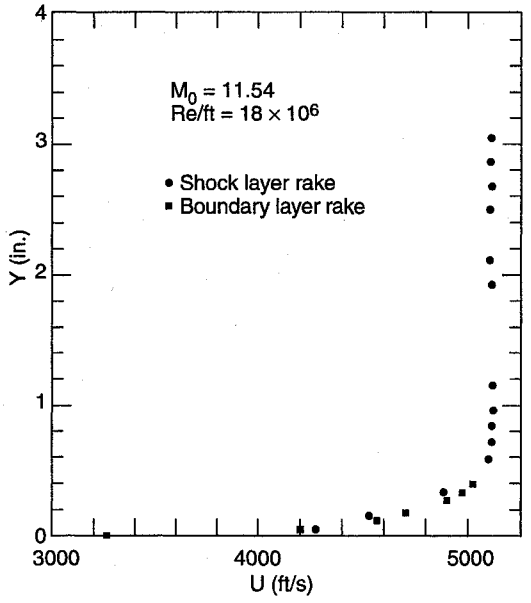

Fig. 7 Velocity distribution at the expansion corner for simple flow over the flat plate.

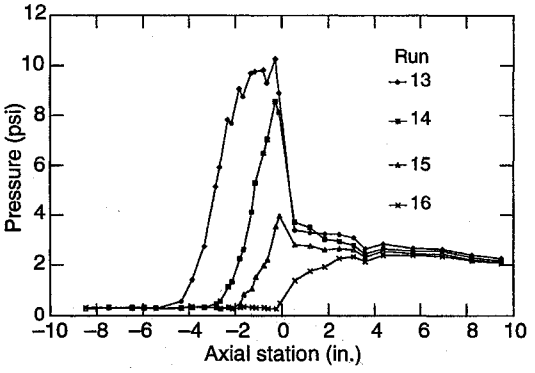

Fig. 8 Pressure distribution for the 10-deg shock generator.

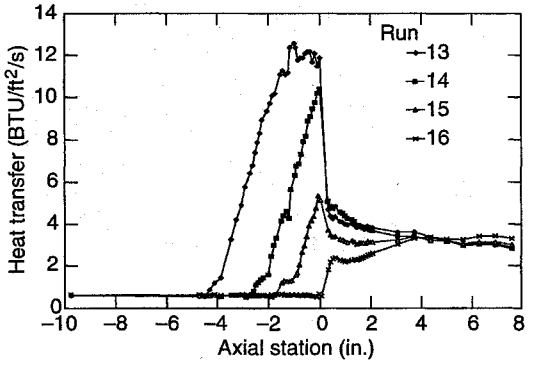

Fig. 9 Heat transfer distribution for the 10-deg shock generator.

shock patterns is quite different in that taking the full shock reflection and then expanding to the final pressure results in significantly higher total pressure loss than shock cancellation at the shoulder.

The heat transfer distributions for the 10-deg shock-generator runs are shown in Fig. 9. The same characteristic curves are evident in these plots; however, there is a significantly higher density of heat transfer gauges. This helps in interpreting some of the key flowfield features relating to the shock interaction with the boundary layer. As evidenced by both the inflection in the pressure distributions and the plateau in the heat transfer curves, there is a small amount of boundary-layer separation for shock impingement points upstream of the shoulder. Even with this small amount of separation, it is not until the separated region reaches the shoulder that there is any appreciable reduction in the size of the separation because of the pressure relief at the shoulder.

The pressure and heat transfer distributions for the 12-deg shock generator are shown in Figs. 10 and 11, respectively. Considerably more runs were made for the 12-deg shock generator in an attempt to better understand the interactions for shock impingement points upstream and downstream of the shoulder. The full reflected shock pressure rise resulted in a pressure ratio of approximately 52:1. The separation region is considerably larger, as evidenced by the more pronounced inflection in the pressure distribution and the larger plateau in the heat transfer distribution. Again, even with a considerable reduction in the pressure ratio that results as the shock position approaches the corner (down to 15:1), the size of the separation region is not affected if the downstream edge of that separation is still upstream of the shoulder.

The pressure and heat transfer distributions for the 15-deg shock angle runs are presented in Figs. 12 and 13, respectively.

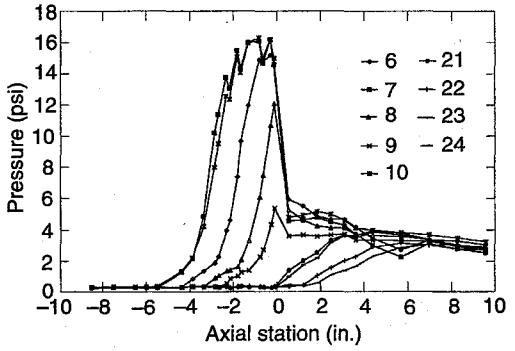

Fig. 10 Pressure distribution for the 12-deg shock generator.

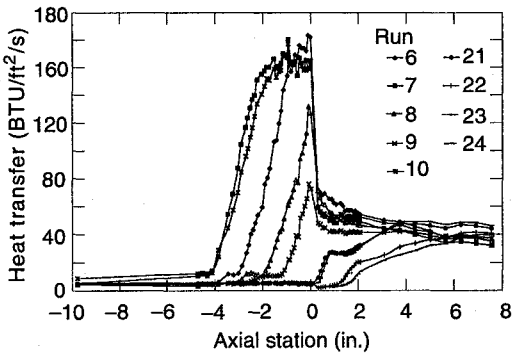

Fig. 11 Heat transfer distribution for the 12-deg shock generator.

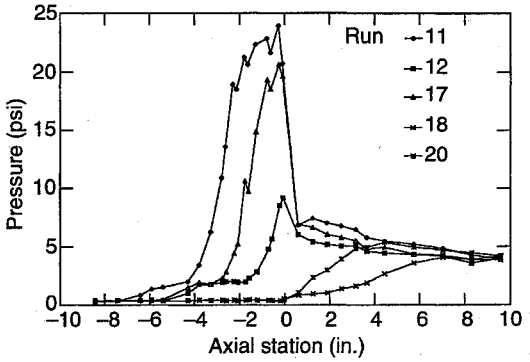

Fig. 12 Pressure distribution for the 15-deg shock generator.

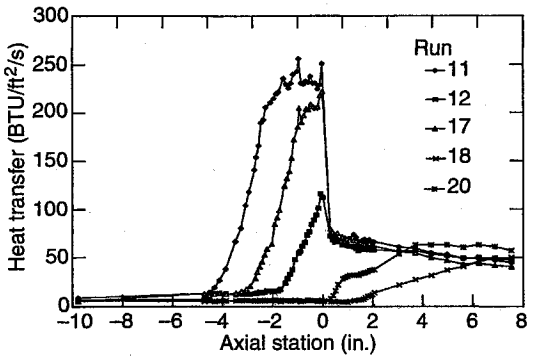

Fig. 13 Heat transfer distribution for the 15-deg shock generator.

For these runs the full reflected shock pressure rise is approximately 84:1, and there is a large region of boundary-layer separation evident for all cases where shock impingement occurs upstream of the shoulder. Moving the shock impingement point toward the corner resulted in a significant reduction in the peak pressure, but once again, the separated region is unaffected if the separation is fully contained upstream of the shoulder.

Summary of Observations

Several general observations and conclusions can be made on the basis of the data generated in this test program, and they are summarized as follows:

1) The pressure data indicate that, depending on the size of the separation, 5–8 boundary-layer heights are required to realize the full pressure rise expected behind the oblique shock reflection.

2) Heat transfer measurements provided a more sensitive indication of separation than pressure measurements for the hardware configuration and instrumentation density utilized in this test program.

3) Relief of the full reflected shock pressure rise begins when the start of the pressure rise is 4–10 boundary-layer heights upstream of the corner.

4) Reduction in the size of separated regions does not occur until the downstream edge of the separated region is very near the expansion corner.

5) Incipient separation appears to occur for a shock-generator angle of 10 deg.

6) Detailed data have been generated for hypersonic shock wave/turbulent interactions in the vicinity of an expansion corner for comparison with solutions generated using computational methods.

Acknowledgments

This article and the analysis of the results presented herein were done under a Stuart S. Janney Fellowship at the Johns Hopkins University Applied Physics Laboratory. The experimental program was conducted under sponsorship of the National Aerospace Plane Joint Program Office in Dayton, Ohio, during the Technology Maturation Plan phase of the NASP program. Technical sponsors for the effort included Edward S. Gravlin, Curtis D. Snyder, and F. Don Stull. The authors are indebted to Michael S. Holden at Calspan for his cooperation during planning and execution of the test program.

References

[1]Waltrup, P. J., White, M. E., and Van Wie, D. M., "Engine Operation and Key Technical Issues in High Speed Propulsion for the National Aerospace Plane," *APL Technical Review*, Vol. 2, No. 1, 1990 (ITAR Restricted).

[2]Delery, J., "Shock/Shock and Shock/Boundary Layer Interactions in Hypersonic Flows," Special Course, Aerothermodynamics of Hypersonic Vehicles, AGARD-FDP-VKI, June 1988.

[3]Delery, J., and Marvin, J. G., "Shock-Wave Boundary Layer Interactions," AGARD-AG-280, Feb. 1986.

[4]Chew, Y. T., "Shock Wave and Boundary Layer Interaction in the Presence of an Expansion Corner," *Aeronautical Quarterly*, Vol. 30, Aug. 1979, pp. 506–527.

[5]Chew, Y. T., and Squire, L. C., "The Boundary Layer Development Downstream of a Shock Interaction at an Expansion Corner," Aeronautical Research Council, Rept. ARC-R/M-3839, Aug. 1978.

[6]Hawbolt, R. J., Sullivan P. A., and Gottlieb, J. J., "Experimental Study of Shock Wave and Hypersonic Boundary Layer Interactions near a Convex Corner," AIAA Paper 93-2980, July 1993.

[7]Chung, K. M., and Lu, F. K., "Hypersonic Turbulent Expansion-Corner Flow with Shock Impingement," *Journal of Propulsion and Power*, Vol. 11, No. 3, 1995, pp. 441–447.

[8]Frew, D., Galassi, L., Stava, D., and Azevedo, D., "A Study of Incipient Separation Limits for Shock-Induced Boundary Layer Separation for Mach 6 High Reynolds Flow," AIAA Paper 93-2481, June 1993.

[9]Holden, M. S., "Shock Wave-Turbulent Boundary Layer Interaction in Hypersonic Flow," AIAA Paper 77-45, Jan. 1977.